

# Do ferroelectric nematic liquid crystals really have a huge dielectric permittivity?

Vojko Matko<sup>1</sup>, Ewa Gorecka<sup>2</sup>, Damian Pocięcha<sup>2</sup>, Joanna Matraszek<sup>2</sup> and Nataša Vaupotič<sup>3,4\*</sup>

<sup>1</sup> University of Maribor, Faculty of Electrical Engineering and Computer Science, Koroška 46, 2000 Maribor

<sup>2</sup> University of Warsaw, Faculty of Chemistry, Zwirki i Wigury 101, 02-089 Warsaw, Poland

<sup>3</sup> University of Maribor, Faculty of Natural Sciences and Mathematics, Koroška 160, 2000 Maribor, Slovenia

<sup>4</sup> Jozef Stefan Institute, Jamova 39, 1000 Ljubljana, Slovenia

\*corresponding author: [natasa.vaupotic@um.si](mailto:natasa.vaupotic@um.si)

## Abstract

There is much scientific debate as to whether the newly discovered ferroelectric nematic liquid crystals actually have a huge relative dielectric constant or whether it is just an artefact related to the interpretation of the dielectric spectroscopy measurement results. We show that the interpretation of the dielectric measurements of highly polar liquid crystalline material requires a new model that takes into account both the frequency response of the tested material and the capacitance of the thin surface layers. A proper interpretation of the measurements confirms a huge relative permittivity of the ferroelectric nematic phase, which can even be orders of magnitude larger than the measured apparent values. Furthermore, the value is independent of the cell thickness and the type of surface electrodes.

Ferroelectric nematic ( $N_F$ ) liquid crystalline (LC) phase is a polar phase with the highest possible symmetry ( $C_{\infty v}$ ). Its recent discovery [1,2] immediately attracted a wide research [3–8]. Ferronematic materials, although fluidic, are characterized by a strong order of dipoles resulting in a large spontaneous electric polarization of the order of  $10^{-3}$  to  $10^{-2}$   $\text{Cm}^{-2}$  [2,9,10], very high values of the second order susceptibility and electrooptic coefficients [11–13], giant flexoelectric effect [14] and potential phototunability of dielectric permittivity [15]. These physical properties position ferroelectric nematics as promising candidates for diverse applications, including display technologies, creation of haptic surfaces, development of polar sensors, and are opening new roads to designing photonic structures [13]. Applications became even more viable and promising with the experimental realization of chiral ferroelectric nematic materials [16–19] and synthesis of materials (or their mixtures) having a ferroelectric nematic phase at a room temperature [9,20–22]. Another distinguishing feature of ferroelectric nematics is their remarkably high relative permittivity, a parameter that quantifies the reduction in the electric field strength inside a material compared to a vacuum and serves as a measure of the material's ability to store electrical energy. Typically measured values of the relative permittivity of a ferroelectric nematic are of the order of  $10^4$ , within a frequency range which can extend up to the kHz regime [2,10,12,23–27]. This huge permittivity has been primarily attributed to the ease with which thermally activated fluctuations of the polarization direction occur. However, the relative permittivity in the ferroelectric nematic phase appears to be strongly influenced by the surface treatment applied to the cells (polymer anchoring layers) in which the dielectric measurements are performed and the thickness of cells [23–27]. A similar effect has been well-documented also in ferroelectric smectic C liquid crystals [28] and in the orthogonal ferroelectric smectic A phases [29] and has been explained by constrains of polar fluctuations by interactions with cell surfaces. However, since for the ferroelectric nematic phase the effect is observed also in very thick cells, in which the surface interactions should be negligible, this raises doubts about the interpretation of the dielectric measurements and poses a question

whether these materials are indeed characterized by large permittivity. Clark et al. suggested [30] that liquid crystalline materials with very high spontaneous polarization behave as a perfect conductor and large apparent dielectric permittivity values are detected because the measured capacitance is, in fact, the capacitance of very thin surface layers of surfactant, which is misinterpreted as a capacitance of the whole cell. On the other hand, the relaxation time of the apparent permittivity is a relaxation time of an equivalent electric circuit including a serial connection of a surface layer capacitor and liquid crystal which, in the ferroelectric nematic phase, behaves as a resistor with ohmic resistivity of the order of  $10^2 \Omega$ . Vaupotic et al. [23] pointed out that in the case of the dielectric strength being very large, the capacitance of the LC becomes comparable to the capacitance of the surface alignment layer thus both the LC capacitor and the surface layer capacitor are charged (as opposed to charging only the surface layer capacitor as proposed by Clark et al.). It was shown that in this case the interpretation of the dielectric response becomes very complex (as noticed also by Yadav et al. [27]), so they focused on the dielectric measurements in cells with no alignment layers for which they assumed that only the capacitance of the LC cell is measured. On the other hand, Yadav et al. [27] studied the response in planar cells with homeotropic and planar alignment as a function of cell thickness and the thickness of the alignment layer, but limited the study primarily to the upper temperature N or N<sub>x</sub> [31] phase in which the charging of the surface layer can be neglected. Erkoreka et al. [24] performed a systematic investigation of the dielectric response as a function of the cell thickness. Their results are interpreted within the model of Clark and within a continuous phenomenological model proposed by Vaupotic et al, which couples fluctuations of the director and polarization. They also considered the possibility of the electrode polarization effect [32], but ruled it out by further investigations [25]. The latter investigations also led to observations of high frequency relaxation processes predicted by the continuous phenomenological model thus confirming that relaxation processes within the N<sub>F</sub> phase are essentially measured by the dielectric spectroscopy, not only the response of the surface layers.

Although the recent dielectric measurements confirm the relaxation modes predicted by a phenomenological model of the N<sub>F</sub> phase, the increase of the dielectric strength with increasing thickness also in very thick cells “rings the bell”, even though some possible explanations have been given [24]. Thus, we decided to perform measurements of a current through and voltage on a parallel plate capacitor filled with a standard ferroelectric nematic liquid crystalline material. These raw measurements were then interpreted in view of different equivalent circuits, also (and especially) such that are not incorporated (yet) in the impedance analyzers used in the so far reported research. The measurements were performed with a simple experimental setup to avoid any possible artefacts. In this letter we show that modelling the LC capacitor as a combination of a capacitor due to surface layers (important even in cells with no polymer alignment layers) and LC capacitor with a frequency dependent dielectric constant allows us to demonstrate that the dependence of the material permittivity on the sample thickness is apparent, and the measurements in different cells (different thickness, different types of electrodes) can be fitted by using the same set of material parameters.

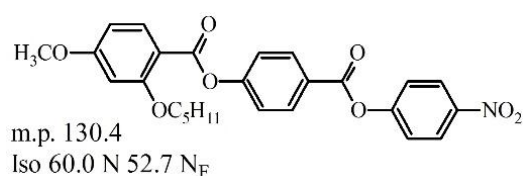


**Figure 1.** Chemical formula of the studied material with phase transition temperatures in °C.

To perform measurements, we used a standard material (analogue of RM734 [1]) (**Figure 1**) exhibiting a metastable nematic and ferronematic phases upon cooling from the isotropic liquid (see **I-5** in ref. [18]). Material was filled in planar cells (capacitors) with gold or indium tin oxide (ITO) electrodes. The cells with gold electrodes were without surface alignment layers, while the cells with ITO electrodes

were either without a surface alignment layer or with a surface polymer alignment layer enforcing homeotropic anchoring. Information on the used cells is collected in **Table 1**. To make sure that systematic tendencies are observed, measurements were also performed for another ferroelectric nematic material (see Supplemental Material, SM).

**Table 1.** Used cells (capacitors), their acronyms, thickness ( $d$ ), capacitance of an empty cell ( $C_0$ ) and surface area of the electrodes ( $S$ ). The low frequency capacitances ( $C$ ) of cells (at 10 Hz) and capacitances per unit surface area ( $C/S$ ) for material in the  $N_F$  phase at 49.0°C. AL stands for alignment layer.

cell	acronym	$d$ [ $\mu\text{m}$ ]	$C_0$ [pF]	$S$ [ $\text{mm}^2$ ]	$C$ [ $\mu\text{F}$ ]	$C/S$ [ $\text{nF mm}^{-2}$ ]
Gold electrodes	G5	5	44	25	0.32	13
	G10	10	22	25	0.25	10
ITO, no AL	NA3	3,0	485	164	2.5	15
	NA5	4,9	95	53	0.52	9.8
	NA10	9,7	150	164	1.9	12
ITO, homeotropic AL	HT10	10,0	77	87	0.29	3.3
	HT20	20,0	41.5	94	0.18	1.9

To obtain the frequency dependence of the real and imaginary part of the impedance of cells filled with the material in the ferronematic phase, we measured a voltage on the cell and phase angle between the voltage on the cell and the applied (generator) voltage (Bode plot method) and, for some cells, also the current through the cell and phase lag between the current and the voltage on the cell (auto-balancing bridge method). Details on both methods are given in SM, where we also give a procedure for calculating the impedance of the cell ( $Z$ ) and the phase angle ( $\alpha$ ) between the voltage on and current through the cell from the measured quantities. The auto-balancing bridge method gives better results (less noise) but it could be used only for low enough frequencies (up to approximately 20 kHz). The Bode plot method gives reliable results up to few MHz and measurements were performed up to 1 MHz, so, primarily, we used the Bode plot method. For signal generation, Siglent SDG6022X 200MHz Function / Arbitrary Waveform Generator (16 bit) was used and measurements were recorded by a Siglent SDS6054A 4CH 500MHz 5 GSa/s Oscilloscope (16 bit). The amplitude of the generator output voltage was set to 100 mVpp for all cells, much below the Frederick's transition voltage. Measurements were repeated also for 200 mVpp and the only effect was less noise at lower frequencies. For few cells, results for the calculated apparent dielectric loss and relative permittivity were compared with the ones obtained by the Solatron 1260 impedance analyzer and a full agreement was obtained. Cells were heated by using a PCB Heating platform HPB100 from iTECH and temperature was measured by a PT100 temperature sensor. The temperature was stabilized with an accuracy of 0.1 K. The oscilloscope enables 4-channel measurements. One channel is required for the function generator, the rest can be used to measure simultaneously three cells, for which the experimental conditions were thus identical.

The impedance  $Z$  and phase angle  $\alpha$  obtained from the measurements of the voltage on the cell and phase angle between the voltage on the cell and the applied voltage (Bode plot method) are given in **Figure 2a,b**, raw data are presented in SM (**Figure S2**). SM also includes measurements by auto-balancing bridge method. The impedance  $Z$  and phase angle  $\alpha$  are obtained from the measured data without making any assumptions on the structure of the cell. From this point on, assumptions are needed to obtain the dielectric loss and relative permittivity of the LC in the  $N_F$  phase. To get some information on a proper equivalent electric circuit of the cell filled with a ferroelectric material, we first interpret the measured impedance ( $Z$ ) and phase angle  $\alpha$  as if resulting from a capacitor and resistor in either a series or parallel connection. A comparison of the frequency dependence of  $\alpha$  (**Figure 2a**) to the dependence that an ideal ohmic resistor and capacitor in series or parallel connection would give (**Figure S7**) makes it very clear that the cell is neither. If the model of Clark et al. was valid, the equivalent electric circuit

would be a series connection of a capacitor due to surface layers and an ohmic resistor due to the resistivity of LC between the surface layers, and the capacitance and resistivity should be constant over the measured frequency range. **Figure 2cd** gives the capacitance ( $C_S$ ) and resistivity ( $R_S$ ) calculated from the measured  $Z$  and  $\alpha$  by interpreting them as coming from a series connection of a capacitor and resistor. We observe that the values are frequency dependent, and the resistivity is rather high, between  $1\text{ k}\Omega$  and  $10\text{ k}\Omega$ , much larger than few  $100\ \Omega$  predicted by Clark et al. In addition, from the model of Clark et al. it follows that one should measure the same capacitance per unit surface of the capacitor for all cells with the same type of electrodes and surface alignment layer, because the capacitance would depend only on the thickness of the surface layer. The low frequency capacitance of all the cells with the material being in the ferroelectric phase is given in **Table 1**. The capacitances per unit surface differ and they are not in the ratio of thicknesses.

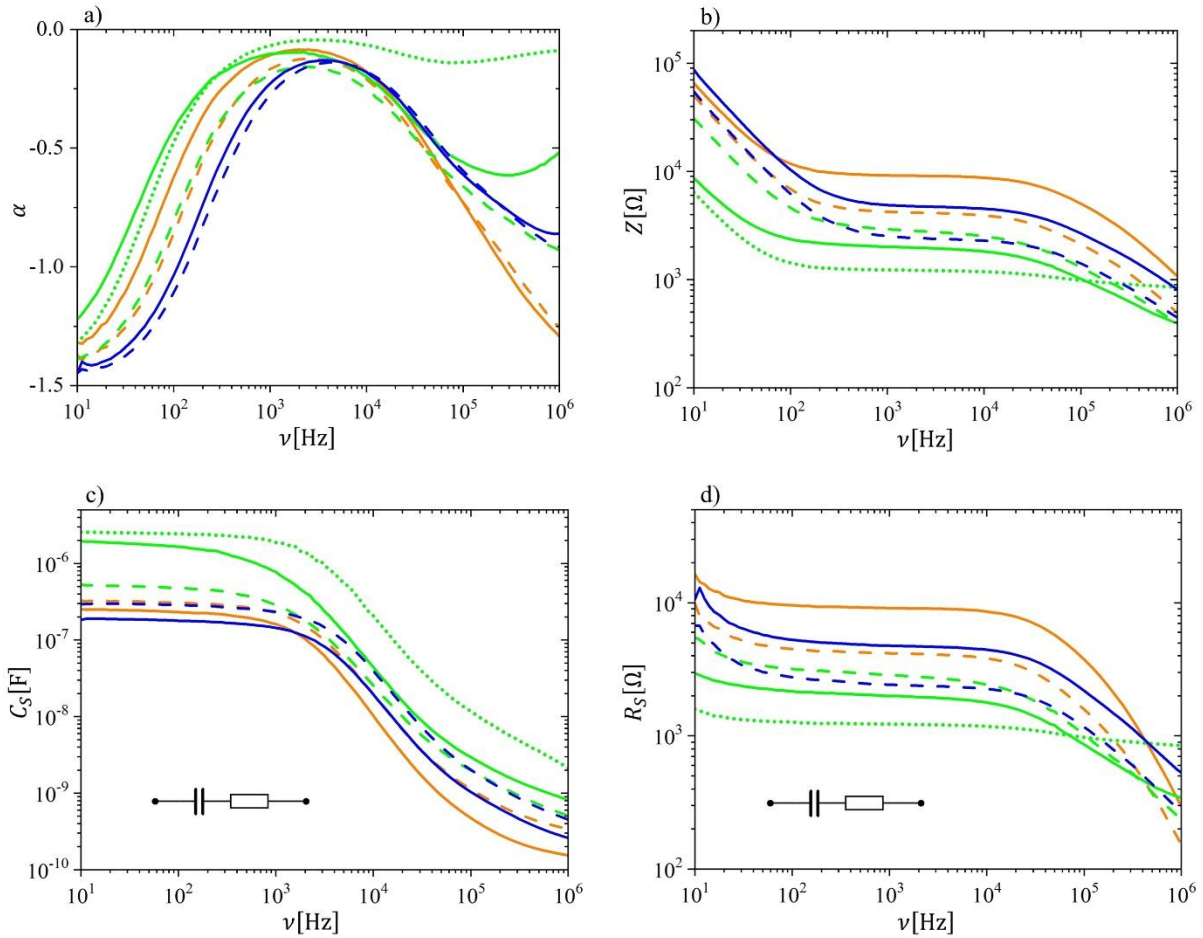


**Figure 2.** a) The phase angle ( $\alpha$ ) between the current through the cell and voltage on the cell and b) impedance ( $|Z|$ ) calculated from the Bode plot measurements for the studied material in the  $N_F$  phase at  $49.0^\circ\text{C}$ . The apparent c) capacitance ( $C_S$ ) and d) resistivity ( $R_S$ ) of the cell as a function of frequency ( $\nu$ ) obtained by simulating the measured  $Z$  and  $\alpha$  as resulting from a series connection of an ideal resistor and capacitor. Green: NA10 (solid), NA5 (dashed), NA3 (dotted). Orange: G10 (solid), G5 (dashed). Blue: HT20 (solid), HT10 (dashed).

The above observations rule out the model of Clark et al.; however, they show that the influence of dielectric layers cannot be neglected, not even in cells without polymer alignment layers on electrodes, where a thin layer of liquid crystal molecules close to the surface behaves as a surface layer, as pointed out by Clark et al. [30]. Because observations of several modes in the dielectric response make it clear that relaxations of the LC material in the cell are also detected, this stimulated us to analyze in more detail an equivalent circuit model which considers both the capacitance of the surface layer as well as the frequency response of the liquid crystalline material (see SM in Ref. [23]). The assumed equivalent

electric circuit is given in **Figure 3**. The capacitance of the surface dielectric layer is  $C_D$ ; there are two surface layers and, assuming that they have a very high ohmic resistivity, their net capacitance is  $C_D/2$ . The capacitance of the liquid crystal ( $C_{LC}$ ) is expressed as

$$C_{LC} = C_0 \varepsilon(\omega), \quad (1)$$

where  $C_0$  is a capacitance of an empty cell and  $\varepsilon(\omega)$ , where  $\omega = 2\pi\nu$ , is a dielectric constant, which we approximate by the Debye relaxation model:

$$\varepsilon(\omega) = \varepsilon'(\omega) + i\varepsilon''(\omega) = \varepsilon_\infty + \frac{\Delta\varepsilon}{1 + i\omega\tau}, \quad (2)$$

$\varepsilon'$  is relative permittivity and  $\varepsilon''$  dielectric loss,  $\varepsilon_\infty$  is a dielectric constant at high frequencies,  $\Delta\varepsilon$  a dielectric strength and  $\tau$  the Debye relaxation time. Havriliak – Negami equation [33] could be used instead, but to show the principle and have a lower number of fitting parameters we decided on the Debye relaxation. The ohmic resistivity of the liquid crystalline material is  $R_{LC}$ . Compared to the equivalent circuit in [23], a resistor with resistivity  $R_x$  is included to describe a decrease in  $\alpha$  at frequencies higher than approximately 10 kHz, see **Figure 2a**. This effect comes from parasitic resistivities of electrodes and wiring. When  $C_D \gg C_{LC}$ ,  $R_{LC}$  is large and  $R_x$  small, only the LC capacitor is charged and by finding the current through the cell that is in phase with the voltage on the cell one actually measures the quantity that is directly proportional to the dielectric loss ( $\varepsilon''$ ). However, the analysis becomes tricky when  $C_D$  and  $C_{LC}$  are comparable. In Ref. [23] we argued that the capacitance of surface layers is important only in cells with surfactants; however, as can be concluded already from the capacitance per unit surface given in **Table 1**, the capacitance of surface dielectric layer must be considered also in cells with no surface polymer anchoring layers.

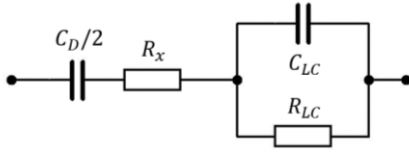


**Figure 3.** The equivalent electric circuit of the cell filled with a ferroelectric liquid crystal.  $C_D$  is the capacitance of one surface layer,  $C_{LC}$  is the capacitance and  $R_{LC}$  resistivity of a liquid crystal.  $R_x$  is a parasitic resistivity.

We searched for such values of the model parameters that would give at least a semi-quantitative fit with the measured results. The major objective was to find a set of LC parameters ( $\Delta\varepsilon$ ,  $\tau$ ,  $\varepsilon_\infty$ ) that are common for all cells regardless of their thickness and type of surface anchoring, because all cells are filled with the same material. We point out that the lower frequency part of experimental results can be fitted even if we use equivalent circuits presenting the LC cell as (i) a capacitor  $C_D$  and resistor  $R_{LC}$  in series, or (ii) a capacitor  $C_{LC}(\omega, \tau)$  and resistor  $R_{LC}$  in parallel. However, it would require a different set of material parameters for each cell. The equivalent circuit in **Figure 3** is the simplest one that enables the description of experimental measurements with the same set of material parameters for all cells. In search for this set of parameters we observed that the physical quantities that are most sensitive to the change of parameter values are  $\alpha(\omega)$  and the apparent dielectric loss ( $\varepsilon''_{AP}$ ) defined as

$$\varepsilon''_{AP} = \frac{I_{in\ phase}}{\omega C_0 U_{cell}}, \quad (3)$$

where  $I_{in\ phase}$  is the current through the cell in phase with the voltage on the cell ( $U_{cell}$ ).

The apparent dielectric loss calculated from the measured data by using eq. (3) is given in **Figure 4a** for all the studied cells. We see that the maximum apparent value of  $\varepsilon''_{AP}$  strongly depends on the cell thickness and on the type of the cell (NA, G or HT). This dependence is an artefact of a huge dielectric strength of the ferroelectric nematic, due to which the condition  $C_D \gg C_{LC}$  is not satisfied any more. In

this case, the maximum of  $\varepsilon''_{AP}$  as given by eq. (3) is not half the value of  $\Delta\varepsilon$ , neither is the position of the peak at a frequency equal to  $1/(2\pi\tau)$ .

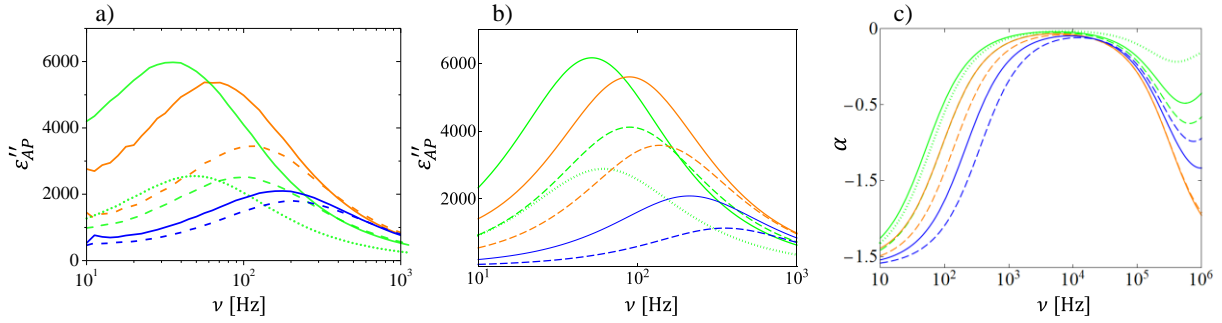


**Figure 4.** a) The frequency dependence of the apparent dielectric loss ( $\varepsilon''_{AP}$ ) for all the studied cells, calculated from the measured data by using eq. (3). Simulated values of b)  $\varepsilon''_{AP}$  and c)  $\alpha$ , calculated for the equivalent circuit given in Figure 3, by taking the material parameter values  $\Delta\varepsilon = 2.5 \cdot 10^4$ ,  $\tau = 4$  ms,  $\varepsilon_\infty = 3$  and  $R_{LC} = 8 \cdot 10^5 \Omega$  being the same for all the cells. The values of  $C_D$  and  $R_x$  which are specific for the type of the cell are given in the main text. Green: NA10 (solid), NA5 (dashed), NA3 (dotted). Orange: G10 (solid), G5 (dashed). Blue: HT20 (solid), HT10 (dashed).

**Figure 4b** gives the apparent dielectric loss as predicted for the model equivalent circuit (Fig. 3) of the LC cell. The plots are obtained for  $\Delta\varepsilon = 2.5 \cdot 10^4$ ,  $\tau = 4$  ms,  $\varepsilon_\infty = 3$  and  $R_{LC} = 8 \cdot 10^5 \Omega$  for all cells, while the thickness of the surface layer, and thus its capacitance and the parasitic resistivity depend on the type of the cell. All cells of the same type (NA, G or HT) were fitted with the same  $R_x$  and the same thickness of the surface layer. The capacitance of the surface layer was modelled as  $C_D = C_0 d f_s$ , where  $f_s = \varepsilon_S/d_S$  and  $d_S$  is a thickness of the surface layer and  $\varepsilon_S$  is its relative permittivity. The plots are given for  $f_s$  being  $5 \text{ nm}^{-1}$  and  $4 \text{ nm}^{-1}$  in the NA and G cells, respectively, while for the HT cells  $f_s = 0.6 \text{ nm}^{-1}$ . These values are physically sensible as one would expect the surface layer to have approximately the same thickness in cells with no aligning surface layer (NA and G cells). In HT cells the surface dielectric layer is found to be of the order of magnitude thicker. By taking  $\varepsilon_S \sim 10$ , we find that  $d_S \sim 2 - 3 \text{ nm}$  in the NA and G cells, while in HT cells  $d_S \approx 17 \text{ nm}$ . While the position and magnitude of the peak value of the apparent  $\varepsilon''_{AP}$  are strongly sensitive to  $\Delta\varepsilon$ ,  $\tau$ ,  $R_{LC}$  and  $f_s$ , the major effect of  $\varepsilon_\infty$  and  $R_x$  is on the higher frequency dependence of the angle  $\alpha$ . A reduction in  $R_x$  increases the magnitude of  $\alpha$  at high frequencies, while the increase in  $\varepsilon_\infty$  shifts the peak (the lowest magnitude of  $\alpha$ ) to lower frequencies. The best fit (compare **Figures 2a and 4c**) was obtained for  $R_x = 600 \Omega$  for the NA cells,  $R_x = 500 \Omega$  for the HT cells and  $R_x = 50 \Omega$  for the G cells. These parameter values make sense, as it is expected that the parasitic resistivity should be the lowest for the cells with gold electrodes.

By considering, that the inaccuracy in the cell thickness and in the filling of the cell can lead to capacitances of cells to differ by up to 10% from the ideal values, we conclude that the proposed equivalent circuit gives not only good qualitative but also semi-quantitative agreement with the experiment. The agreement between the model predictions and measurements is obtained only if very high  $\Delta\varepsilon$  is assumed, which is approximately four times higher than the maximum of the apparent dielectric loss measured in the NA10 cell. The presented model explains why the apparent dielectric strength increases with increasing cell thickness: by increasing the cell thickness, the capacitance  $C_{LC}$  decreases and we are moving towards the limit  $C_{LC} \ll C_D$  in which the apparent dielectric strength and loss coincide with the actual material parameters (**Figure S3**). If we use the obtained parameters to estimate  $C_{LC}$  and  $C_D$  for different cells we obtain  $C_{LC} \approx 0.6 C_D \approx 0.5 \mu\text{F}$  for G10 cell,  $C_{LC} \approx 4 C_D \approx 2 \mu\text{F}$  for HT10 cell, and  $C_{LC} \approx 0.5 C_D \approx 3.8 \mu\text{F}$  for NA10 cell, thus the capacitances are indeed comparable. To fulfill the condition  $C_{LC} \ll C_D$  the cell thickness should be of the order of several millimeters, while in standard experiments with LC materials the cells not thicker than approximately  $100 \mu\text{m}$  are used.

However, as shown in SM, for very thick cells, the peak in the dielectric loss at the Debye frequency  $1/2\pi\tau$  might be hidden in the low frequency increase of the dielectric loss.

To conclude, we have shown that the low frequency (up to 1 MHz) response obtained by dielectric measurements of a ferroelectric nematic material filled in thin capacitors can be interpreted in terms of the same material quantities (relative permittivity and relaxation time) independent of the cell thickness and the type of surface electrodes and surface alignment layer. Standard procedure, in which the dielectric loss is calculated from the current through the cell flowing in phase with the voltage on the cell and the relative permittivity - from the current through the cell phase shifted with respect to the voltage by  $\pi/2$ , gives only apparent values, related to material properties in a very complex way. The reason lies in a huge relative permittivity of the LC in the ferroelectric nematic phase, which causes the capacitance of the liquid crystal slab to be comparable to the capacitance of the surface dielectric layer and the latter is shown to exist also in capacitors with bare electrodes. We show that experimental observations can be explained by modelling the LC cell with an equivalent circuit consisting of a series connection of a capacitor due to the surface dielectric layer, resistor due to parasitic resistivities and LC capacitor (with Debye relaxation) and LC resistor in parallel connection. By using the same values of the dielectric strength of the studied material and its relaxation time for all the studied cells, it is shown that the apparent relative permittivity will increase with increasing cell thickness, the apparent relaxation frequency, however, does not necessarily behave in a monotonic way, which is observed experimentally and predicted by the model (see **Figure 4**, graphs for NA cells, and **Figure S3**). Based on the presented findings, we conclude that the relative permittivity of the ferroelectric nematics is indeed huge, and it is even higher than the apparent measured values. Therefore, the interpretation of the dielectric measurements in strongly polar LC phases needs to be revisited. The use of the proposed equivalent circuit for the interpretation of the apparent relative permittivity and apparent relaxation time might affect the observed dependencies of those parameters on temperature and bias field. It could also explain the unusual dependence of the amplitude mode on temperature close to the  $N_F - N$  transition, reported in [23].

## Acknowledgments

N. V. and V.M. acknowledge the support of the Slovenian Research and Innovation Agency (ARIS), through the research core funding program No. P1-0055 and No. P2-0028, respectively. E. G., D. P. and J. M. acknowledge the support by the National Science Centre (Poland) under the grant no. 2021/43/B/ST5/00240.

## References

- [1] R. J. Mandle, S. J. Cowling, and J. W. Goodby, *A Nematic to Nematic Transformation Exhibited by a Rod-like Liquid Crystal*, *Phys. Chem. Chem. Phys.* **19**, 11429 (2017).
- [2] H. Nishikawa, K. Shiroshita, H. Higuchi, Y. Okumura, Y. Haseba, S. Yamamoto, K. Sago, and H. Kikuchi, *A Fluid Liquid Crystal Material with Highly Polar Order*, *Advanced Materials* **29**, 1702354 (2017).
- [3] R. J. Mandle, S. J. Cowling, and J. W. Goodby, *Rational Design of Rod-Like Liquid Crystals Exhibiting Two Nematic Phases*, *Chemistry A European J* **23**, 14554 (2017).
- [4] A. Mertelj, L. Cmok, N. Sebastián, R. J. Mandle, R. R. Parker, A. C. Whitwood, J. W. Goodby, and M. Čopič, *Splay Nematic Phase*, *Phys. Rev. X* **8**, 041025 (2018).
- [5] N. Sebastián, L. Cmok, R. J. Mandle, M. R. De La Fuente, I. Drevenšek Olenik, M. Čopič, and A. Mertelj, *Ferroelectric-Ferroelastic Phase Transition in a Nematic Liquid Crystal*, *Phys. Rev. Lett.* **124**, 037801 (2020).
- [6] X. Chen et al., *First-Principles Experimental Demonstration of Ferroelectricity in a Thermotropic Nematic Liquid Crystal: Polar Domains and Striking Electro-Optics*, *Proc. Natl. Acad. Sci. U.S.A.* **117**, 14021 (2020).

- [7] R. J. Mandle, N. Sebastián, J. Martínez-Perdiguero, and A. Mertelj, *On the Molecular Origins of the Ferroelectric Splay Nematic Phase*, *Nat Commun* **12**, 4962 (2021).
- [8] N. Sebastián, M. Čopič, and A. Mertelj, *Ferroelectric Nematic Liquid-Crystalline Phases*, *Phys. Rev. E* **106**, 021001 (2022).
- [9] E. Zavvou, M. Klasen-Memmer, A. Manabe, M. Bremer, and A. Eremin, *Polarisation-Driven Magneto-Optical and Nonlinear-Optical Behaviour of a Room-Temperature Ferroelectric Nematic Phase*, *Soft Matter* **18**, 8804 (2022).
- [10] M. Cigl, N. Podoliak, T. Landovský, D. Repčák, P. Kužel, and V. Novotná, *Giant Permittivity in Dimethylamino-Terminated Ferroelectric Nematogens*, *Journal of Molecular Liquids* **385**, 122360 (2023).
- [11] C. L. Folcia, J. Ortega, R. Vidal, T. Sierra, and J. Etxebarria, *The Ferroelectric Nematic Phase: An Optimum Liquid Crystal Candidate for Nonlinear Optics*, *Liquid Crystals* **49**, 899 (2022).
- [12] J. Li, H. Nishikawa, J. Kougo, J. Zhou, S. Dai, W. Tang, X. Zhao, Y. Hisai, M. Huang, and S. Aya, *Development of Ferroelectric Nematic Fluids with Giant- $\epsilon$  Dielectricity and Nonlinear Optical Properties*, *Sci. Adv.* **7**, eabf5047 (2021).
- [13] N. Sebastián et al., *Polarization Patterning in Ferroelectric Nematic Liquids via Flexoelectric Coupling*, *Nat Commun* **14**, 3029 (2023).
- [14] A. Barthakur, J. Karcz, P. Kula, and S. Dhara, *Critical Splay Fluctuations and Colossal Flexoelectric Effect above the Nonpolar to Polar Nematic Phase Transition*, *Phys. Rev. Materials* **7**, 035603 (2023).
- [15] H. Nishikawa, K. Sano, and F. Araoka, *Anisotropic Fluid with Phototunable Dielectric Permittivity*, *Nat Commun* **13**, 1142 (2022).
- [16] H. Nishikawa and F. Araoka, *A New Class of Chiral Nematic Phase with Helical Polar Order*, *Advanced Materials* **33**, 2101305 (2021).
- [17] J. Ortega, C. L. Folcia, J. Etxebarria, and T. Sierra, *Ferroelectric Chiral Nematic Liquid Crystals: New Photonic Materials with Multiple Bandgaps Controllable by Low Electric Fields*, *Liquid Crystals* **49**, 2128 (2022).
- [18] D. Pocięcha et al., *Intrinsically Chiral Ferronematic Liquid Crystals: An Inversion of the Helical Twist Sense at the Chiral Nematic – Chiral Ferronematic Phase Transition*, *Journal of Molecular Liquids* **361**, 119532 (2022).
- [19] C. Feng, R. Saha, E. Korblova, D. Walba, S. N. Sprunt, and A. Jákli, *Electrically Tunable Reflection Color of Chiral Ferroelectric Nematic Liquid Crystals*, *Advanced Optical Materials* **9**, 2101230 (2021).
- [20] A. Manabe, M. Bremer, and M. Kraska, *Ferroelectric Nematic Phase at and below Room Temperature*, *Liquid Crystals* **48**, 1079 (2021).
- [21] X. Chen, Z. Zhu, M. J. Magrini, E. Korblova, C. S. Park, M. A. Glaser, J. E. MacLennan, D. M. Walba, and N. A. Clark, *Ideal Mixing of Paraelectric and Ferroelectric Nematic Phases in Liquid Crystals of Distinct Molecular Species*, *Liquid Crystals* **49**, 1531 (2022).
- [22] H. Long, J. Li, M. Huang, and S. Aya, *Mixing-Induced Phase Stabilization and Low-Temperature-Shifting of Ferroelectric Nematics*, *Liquid Crystals* **49**, 2121 (2022).
- [23] N. Vaupotič, D. Pocięcha, P. Rybak, J. Matraszek, M. Čepič, J. M. Wolska, and E. Gorecka, *Dielectric Response of a Ferroelectric Nematic Liquid Crystalline Phase in Thin Cells*, *Liquid Crystals* **50**, 584 (2023).
- [24] A. Erkoreka, J. Martínez-Perdiguero, R. J. Mandle, A. Mertelj, and N. Sebastián, *Dielectric Spectroscopy of a Ferroelectric Nematic Liquid Crystal and the Effect of the Sample Thickness*, *Journal of Molecular Liquids* **387**, 122566 (2023).
- [25] A. Erkoreka, A. Mertelj, M. Huang, S. Aya, N. Sebastián, and J. Martínez-Perdiguero, *Collective and Non-Collective Molecular Dynamics in a Ferroelectric Nematic Liquid Crystal Studied by Broadband Dielectric Spectroscopy*, *The Journal of Chemical Physics* **159**, 184502 (2023).
- [26] N. Yadav, Y. P. Panarin, W. Jiang, G. H. Mehl, and J. K. Vij, *Collective Relaxation Processes in Nonchiral Nematics*, *Crystals* **13**, 962 (2023).
- [27] N. Yadav, Y. P. Panarin, J. K. Vij, W. Jiang, and G. H. Mehl, *Two Mechanisms for the Formation of the Ferronematic Phase Studied by Dielectric Spectroscopy*, *Journal of Molecular Liquids* **378**, 121570 (2023).

- [28] Yu. P. Panarin, Yu. P. Kalmykov, S. T. Mac Lughadha, H. Xu, and J. K. Vij, *Dielectric Response of Surface Stabilized Ferroelectric Liquid Crystal Cells*, Phys. Rev. E **50**, 4763 (1994).
- [29] L. Guo et al., *Ferroelectric Behavior of Orthogonal Smectic Phase Made of Bent-Core Molecules*, Phys. Rev. E **84**, 031706 (2011).
- [30] N. A. Clark, X. Chen, J. E. Maclennan, and M. A. Glaser, *Dielectric Spectroscopy of Ferroelectric Nematic Liquid Crystals: Measuring the Capacitance of Insulating Interfacial Layers*, (2022).
- [31] X. Chen et al., *The Smectic  $Z_A$  Phase: Antiferroelectric Smectic Order as a Prelude to the Ferroelectric Nematic*, Proc. Natl. Acad. Sci. U.S.A. **120**, e2217150120 (2023).
- [32] S. Emmert, M. Wolf, R. Gulich, S. Krohns, S. Kastner, P. Lunkenheimer, and A. Loidl, *Electrode Polarization Effects in Broadband Dielectric Spectroscopy*, Eur. Phys. J. B **83**, 157 (2011).
- [33] S. Havriliak and S. Negami, *A Complex Plane Analysis of  $\alpha$ -dispersions in Some Polymer Systems*, J. Polym. Sci., C Polym. Symp. **14**, 99 (1966).

Supplemental Materials for:

## **Do ferroelectric nematic liquid crystals really have a huge dielectric permittivity?**

Vojko Matko<sup>1</sup>, Ewa Gorecka<sup>2</sup>, Damian Pocięcha<sup>2</sup>, Joanna Matraszek<sup>2</sup>, Nataša Vaupotič<sup>3,4\*</sup>

- <sup>1</sup> University of Maribor, Faculty of Electrical Engineering and Computer Science, Koroška 46, 2000 Maribor
- <sup>2</sup> University of Warsaw, Faculty of Chemistry, Zwirki i Wigury 101, 02-089 Warsaw, Poland
- <sup>3</sup> University of Maribor, Faculty of Natural Sciences and Mathematics, Koroška 160, 2000 Maribor, Slovenia
- <sup>4</sup> Jozef Stefan Institute, Jamova 39, 1000 Ljubljana, Slovenia

### **Contents:**

- 1 Experimental techniques
- 2 Additional data

# 1 Experimental techniques

Even though the derivations given below are standard calculations known from the elementary course of Physics of measurements in electro engineering, we give them step by step, because in standard measurements with the impedance analyzers one usually does not think about the background “raw” measurements from which the dielectric loss and relative permittivity are calculated based on some assumed equivalent circuit of the LC cell.

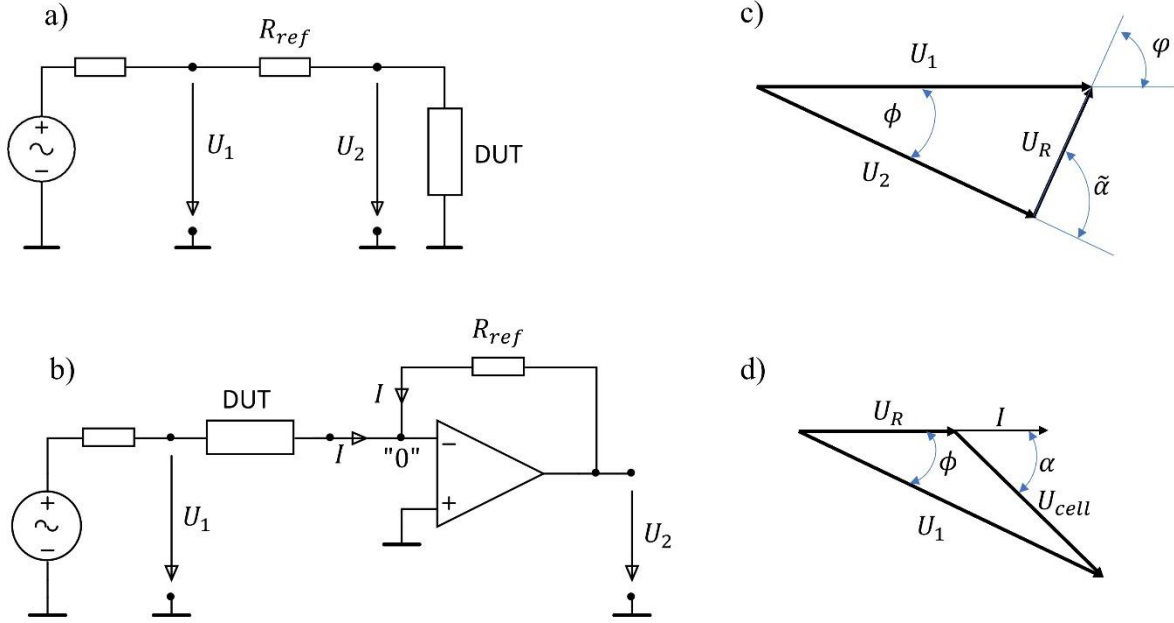


**Figure S1.** Electric circuit for the a) Bode plot and b) auto-balancing bridge method.  $U_1$  is given by the Siglent waveform generator,  $U_2$  is measured by the Siglent oscilloscope,  $R_{ref}$  is resistivity of the reference resistor, DUT is a “device under test”, in our case a series connection of the LC cell and an ohmic resistor with resistivity  $R_c$  used for the compensation of the high frequency response of the probes. c) Phasor diagram for the analysis of the Bode plot method:  $\phi$  is a phase angle between the applied (generator) voltage and the voltage on DUT,  $\varphi$  is the phase angle between the current through DUT and the applied voltage,  $\tilde{\alpha}$  is a phase angle between the voltage on DUT and current through DUT, which is in phase with the voltage  $U_R$  on  $R_{ref}$ . d) Phasor diagram for the auto-balancing bridge method:  $\phi$  is the phase angle between the applied (generator) voltage and current through the cell,  $U_R$  and  $U_{cell}$  are voltages on  $R_c$  and cell, respectively;  $\alpha$  is the phase angle between the voltage on the cell and current ( $I$ ) through the cell.

The schematic circuit of the **Bode plot method** is shown in **Figure S1a**. We measure the voltage ( $U_2$ ) on the device under test (DUT) and the phase angle ( $\phi$ ) between  $U_2$  and voltage ( $U_1$ ) at the generator output. Usually, a gain  $G = 20 \text{ dB} \log(U_2/U_1)$ , is measured, thus  $U_2 = U_1 10^{G/20}$ .

The current through the cell is obtained by calculating the current through the reference resistor as (see the phasor diagram in **Figure S1b**)

$$I = \frac{1}{R_{ref}} \sqrt{U_2^2 + U_1^2 - 2U_2U_1 \cos \phi} . \quad (S1)$$

The phase angle ( $\varphi$ ) between the current through the reference resistor ( $R_{ref}$ ) and the applied voltage is

$$\tan \varphi = \frac{-U_2 \sin \phi}{U_1 - U_2 \cos \phi} \quad (S2)$$

and the phase angle between the voltage on DUT and current through DUT is

$$\tilde{\alpha} = \phi - \varphi . \quad (S3)$$

The impedance of DUT is  $\tilde{Z} = U_2/I$ :

$$\tilde{Z} = \frac{R_{ref} 10^{\frac{G}{20}}}{\sqrt{10^{\frac{G}{10}} + 1 - 2 \cdot 10^{\frac{G}{20}} \cos \phi}} . \quad (S4)$$

We point out that the impedance is independent of the used  $R_{ref}$ , because  $G$  and  $\phi$  also depend on  $R_{ref}$ .

In our measurements, DUT was a series connection of LC cell and a resistor with resistivity  $R_c$ , which was chosen such that a high frequency response of the probes was compensated up to 10 MHz. The measurements on the cells are reliable up to few MHz, for higher frequencies additional effects appear, related probably to parasitic conductance.

If we interpret the measured  $\tilde{Z}$  and  $\tilde{\alpha}$  as being a result of a resistor and capacitor in series, the resistivity ( $R_S$ ) of the LC cell and capacitance ( $C_S$ ) are obtained as

$$R_S = \tilde{Z} \cos \tilde{\alpha} - R_c , \quad C_S = (\tilde{Z} \omega \sin \tilde{\alpha})^{-1} , \quad (S5)$$

where  $\omega = 2\pi\nu$ . The impedance ( $Z$ ) of the LC cell is

$$Z = \sqrt{R_S^2 + (\tilde{Z} \sin \tilde{\alpha})^2} \quad (S6)$$

and the angle between the real and imaginary part of  $Z$  is

$$\tan \alpha = \frac{\tilde{Z} \sin \tilde{\alpha}}{R_S} . \quad (S7)$$

The schematic circuit used for the **auto-balancing bridge method** is shown in **Figure S1c**. We measure the voltage  $U_2$  and the phase angle  $\phi$  between the current ( $I$ ) through DUT and voltage on DUT, the latter being equal to the output generator voltage  $U_1$ . The current through DUT is calculated as

$$I = -\frac{U_2}{R_{ref}} . \quad (S8)$$

Again, DUT is a series connection of a LC cell and resistor with resistivity  $R_c$ , which was added to compensate for the high frequency response of the probes. While for standard ohmic resistors or capacitors the compensation was perfect up to few MHz, we detected increased noise for the LC cells already at frequencies above few 10 kHz. The voltage  $U_1$  on the DUT is a phasor sum of the voltage on  $R_c$  ( $U_R$ ) and on LC cell ( $U_{cell}$ ), see **Figure S1d**, thus  $U_{cell}$  is calculated as

$$U_{cell} = \sqrt{U_1^2 + U_R^2 - 2U_1U_R \cos \phi} . \quad (S9)$$

The angle between the current through the cell and voltage on the cell ( $\alpha$ ) is

$$\tan \alpha = \frac{-U_1 \sin \phi}{U_1 \cos \phi - U_R} . \quad (S10)$$

Because the current through DUT is also the current through the cell, the impedance of the cell is obtained as

$$Z = \frac{U_{cell}}{I} . \quad (S11)$$

If we interpret the measured  $Z$  and  $\alpha$  as resulting from a series connection of a capacitor with capacitance  $C_S$  and resistor with resistivity  $R_S$ , then  $C_S$  and  $R_S$  are calculated as

$$R_S = Z \cos \alpha , C_S = (Z \omega \sin \alpha)^{-1} . \quad (S12)$$

We used  $U_1 = 100$  mVpp in all measurements. The resistivity  $R_{ref}$  was 9,7 k $\Omega$  and 5.1 k $\Omega$  for the Bode plot and auto-balancing bridge method, respectively. The values of  $R_C$  were fitted for each channel and each measurement and were from few 100  $\Omega$  to few k $\Omega$ .

The apparent dielectric loss ( $\varepsilon''_{AP}$ ) is calculated as (eq. (3) in the main text)

$$\varepsilon''_{AP} = \frac{I_{in\ phase}}{\omega C_0 U_{cell}} , \quad (S13)$$

where  $I_{in\ phase}$  is the current through the cell in phase with the voltage on the cell. We note that  $I_{in\ phase} = I \cos \alpha$  and use eq. (S11) to obtain

$$\varepsilon''_{AP} = \frac{\cos \alpha}{\omega C_0 Z} . \quad (S14)$$

## 2 Additional data

In this Section we present the Bode plot measurements of the studied material (**Material 1**) and some additional model results for this material. We also present measurements by the Bode plot method and auto-balancing bridge method of another typical  $N_F$  material (**Material 2**) exhibiting a direct transition from the isotropic to the ferronematic phase at 85°C; measurements were performed at 80°C.

**Figure S2** gives the raw measured data, gain  $G$  and phase angle ( $\phi$ ) between the voltage on DUT (LC cell and  $R_C$  in series) and voltage on the generator output for material 1 in the  $N_F$  phase. From this data we calculated the impedance ( $Z$ ) of the cell and the angle ( $\alpha$ ) between the current through the cell and voltage on the cell as well as  $C_S$  and  $R_S$ . These results are given in Figure 2 of the main text and are to be compared with model results given in **Figure S3**. Model parameters are collected in **Table S1**. In **Figure S3** we also give the apparent dielectric loss as predicted by the model for different cell thicknesses, going beyond the cell thicknesses used in the experiment. We see that by increasing the cell thickness the magnitude and position of the peak value of  $\varepsilon''_{AP}$  move towards the frequency  $1/2\pi\tau$  and magnitude  $\Delta\varepsilon/2$ , as expected. However, at very thick cells the peak is overrun by the low frequency increase of  $\varepsilon''$ . Here, it is worth pointing out that at very low frequencies (below 1 Hz) an ohmic resistor should be added in parallel with the capacitor  $C_D/2$  (see Figure 3), otherwise an additional artificial peak is obtained in the frequency dependence of  $\varepsilon''$  at a frequency  $(\pi C_D R_{RC})^{-1} \sim 0.1$  Hz. Because we are not interested in such low frequencies, the ohmic resistivity of the surface capacitor was assumed to be infinitely large.

Measurements with material 2 were performed only in three cells (based on the availability of the cells): G10, G5 and NA3. For material 2 we present the results both for the Bode plot method (**Figure S4**) and auto-balancing bridge method (**Figure S5**). The apparent dielectric loss ( $\varepsilon''_{AP}$ ) is calculated by eq. (S14). **Figure S6** gives the model predictions. The model parameters are collected in **Table S1**. For this material, the optimum fit is obtained for the following parameter values:  $\varepsilon_\infty = 5$ ,  $\Delta\varepsilon = 3.0 \cdot 10^5$ ,  $\tau =$

0.45 ms and  $R_{LC} = 8 \cdot 10^5 \Omega$ . The values of  $f_S$  are the same for both NA and G cells:  $f_S = 5 \text{ nm}^{-1}$ , the value of  $R_x = 50 \Omega$  for the gold cells is the same as for Material 1, but the model curves are very weakly dependent on lowering this value below 50  $\Omega$ . For the NA3 cell, however, the position of the peak  $\epsilon''_{AP}$  depends strongly on  $R_x$  and the best fit is found for  $R_x = 200 \Omega$ , i.e. a few times lower than for material 1 but still of the same order of magnitude. With these parameters the model predicts a monotonic increase of the maximum apparent dielectric loss with cell thickness, both for the G and NA cells. On the other hand, apparent relaxation frequency decreases towards the LC Debye relaxation frequency with increasing cell thickness in G cells, while in NA cells it increases towards this value.

Finally, in **Figure S7** we consider a parallel and series connection of a resistor with resistivity 1 k $\Omega$  and capacitor with capacitance 1  $\mu\text{F}$  and plot the graphs of  $\alpha$  and  $Z$  for both connections. These graphs are to be compared with  $\alpha$  and  $Z$  obtained from the experiment.

**Table 2.** Model parameters. Their definition is given in the main text.

material	$\Delta\epsilon$ [ $\times 10^4$ ]	$\tau$ [ms]	$\epsilon_\infty$	$R_{LC}$ [ $M\Omega$ ]	$f_s^{(G)}$ [ $\text{nm}^{-1}$ ]	$f_s^{(NA)}$ [ $\text{nm}^{-1}$ ]	$f_s^{(HT)}$ [ $\text{nm}^{-1}$ ]	$R_x^{(G)}$ [ $\Omega$ ]	$R_x^{(NA)}$ [ $\Omega$ ]	$R_x^{(HT)}$ [ $\Omega$ ]
1	2.5	4.0	3	0.8	4	5	0.6	50	600	500
2	3.0	0.45	5	0.8	5	5	/	50	200	/

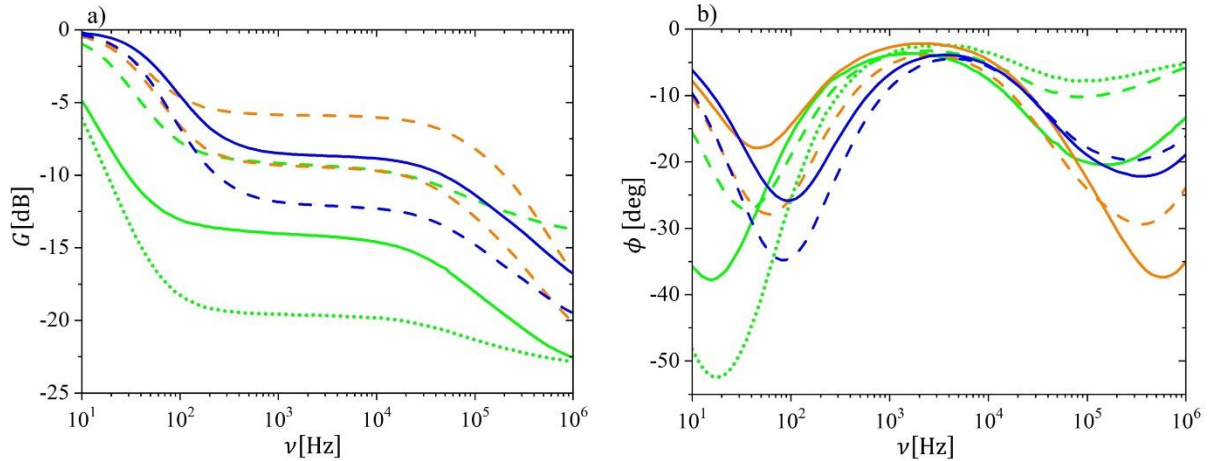


**Figure S2. Material 1** in the  $N_F$  phase at 49.0°C. **Bode plot measurements.** a) Gain ( $G$ ) and b) phase angle ( $\phi$ ) between the voltage on DUT (LC cell and  $R_c$  in series) and voltage on the generator output. Green: NA10 (solid), NA5 (dashed), NA3 (dotted). Yellow: G10 (solid), G5 (dashed). Blue: HT20 (solid), HT10 (dashed).

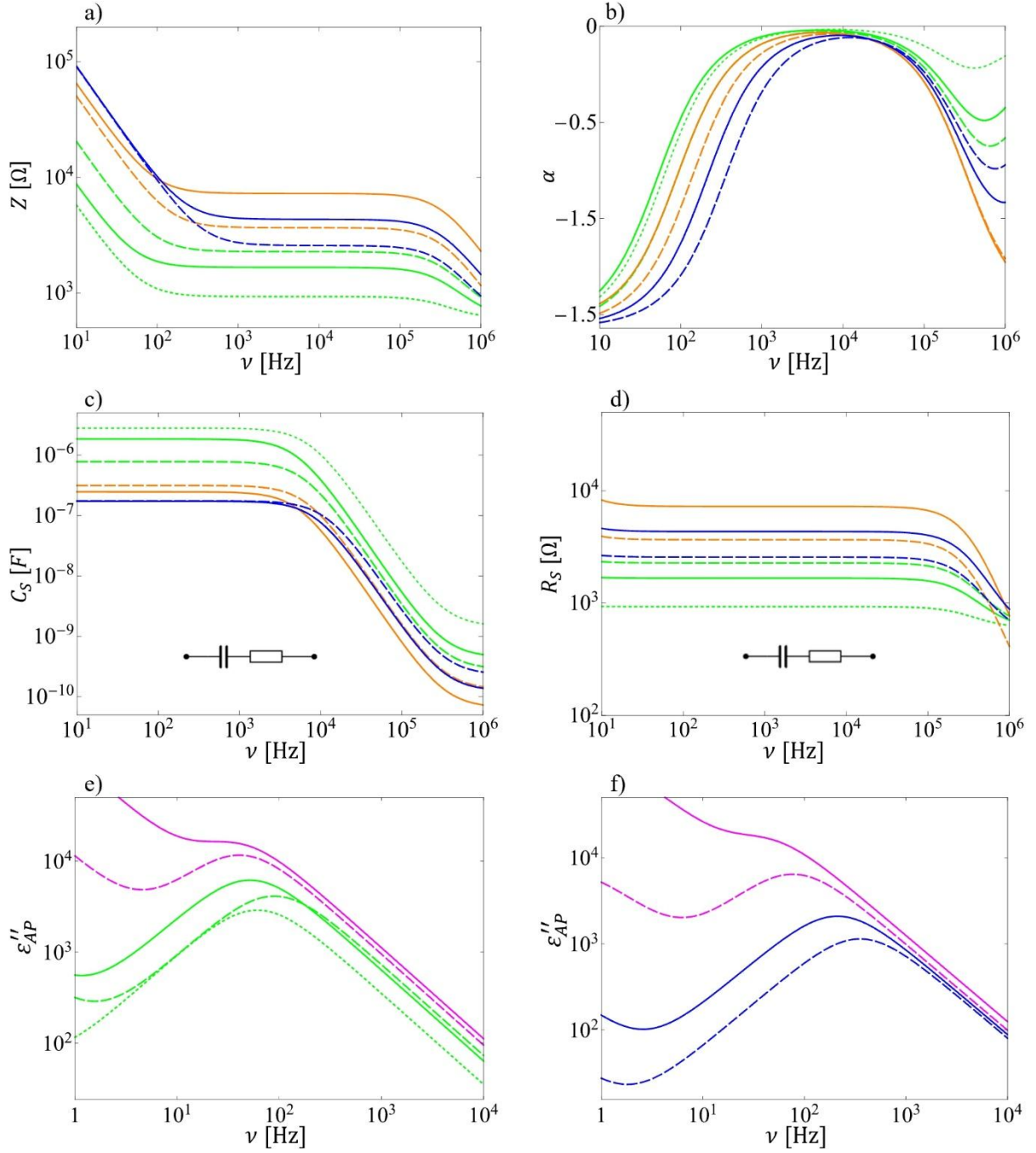


**Figure S3. Material 1. Model results.** a) The impedance ( $Z$ ) and b) phase angle ( $\alpha$ ) between the current through the cell and voltage on the cell as a function of frequency ( $\nu$ ), calculated for the equivalent circuit of the LC cell (Figure 3) with parameters given in Table S1. The apparent c) capacitance ( $C_S$ ) and d) resistivity ( $R_S$ ) of the cell obtained by simulating  $Z$  and  $\alpha$  of the equivalent circuit as if resulting from a series connection of a resistor and capacitor (to be compared with experimental results in Figure 2). An apparent dielectric loss ( $\epsilon''_{AP}$ ) at different cell thicknesses for the e) NA and f) HT cells. Here the green and blue curves present the model results for the studied cells, and magenta curves for 100 nm (dashed curve) and 1 mm (solid curve) thick cell. Green: NA10 (solid), NA5 (dashed), NA3 (dotted). Orange: G10 (solid), G5 (dashed). Blue: HT20 (solid), HT10 (dashed).

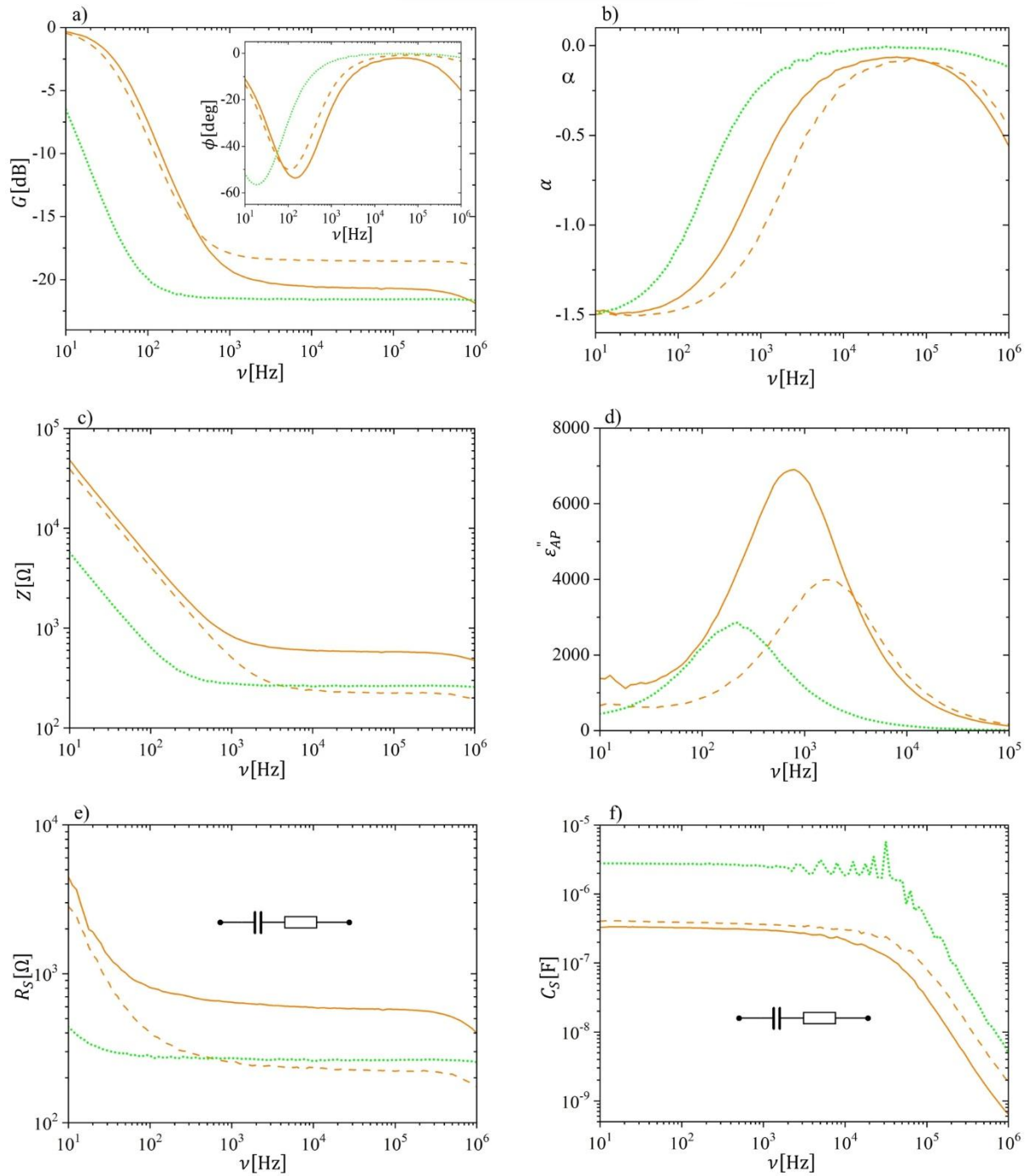


**Figure S4. Material 2** in the  $N_F$  phase at  $80.0^\circ\text{C}$ . **Bode plot measurements.** a) Gain ( $G$ ) and (inset) phase angle ( $\phi$ ) between the voltage on DUT (LC cell and  $R_c$  in series) and voltage on DUT. b) Phase angle ( $\alpha$ ) between the current through the cell and voltage on the cell and c) impedance  $Z$  calculated from  $G$  and  $\phi$ . d) The apparent dielectric loss calculated by eq.(S14). The apparent e) resistivity ( $R_S$ ) and f) capacitance ( $C_S$ ) of the cell as a function of frequency ( $\nu$ ) by simulating the measured  $Z$  and  $\alpha$  as resulting from a series connection of an ideal resistor and capacitor. Green: NA3. Orange: G10 (solid), G5 (dashed).

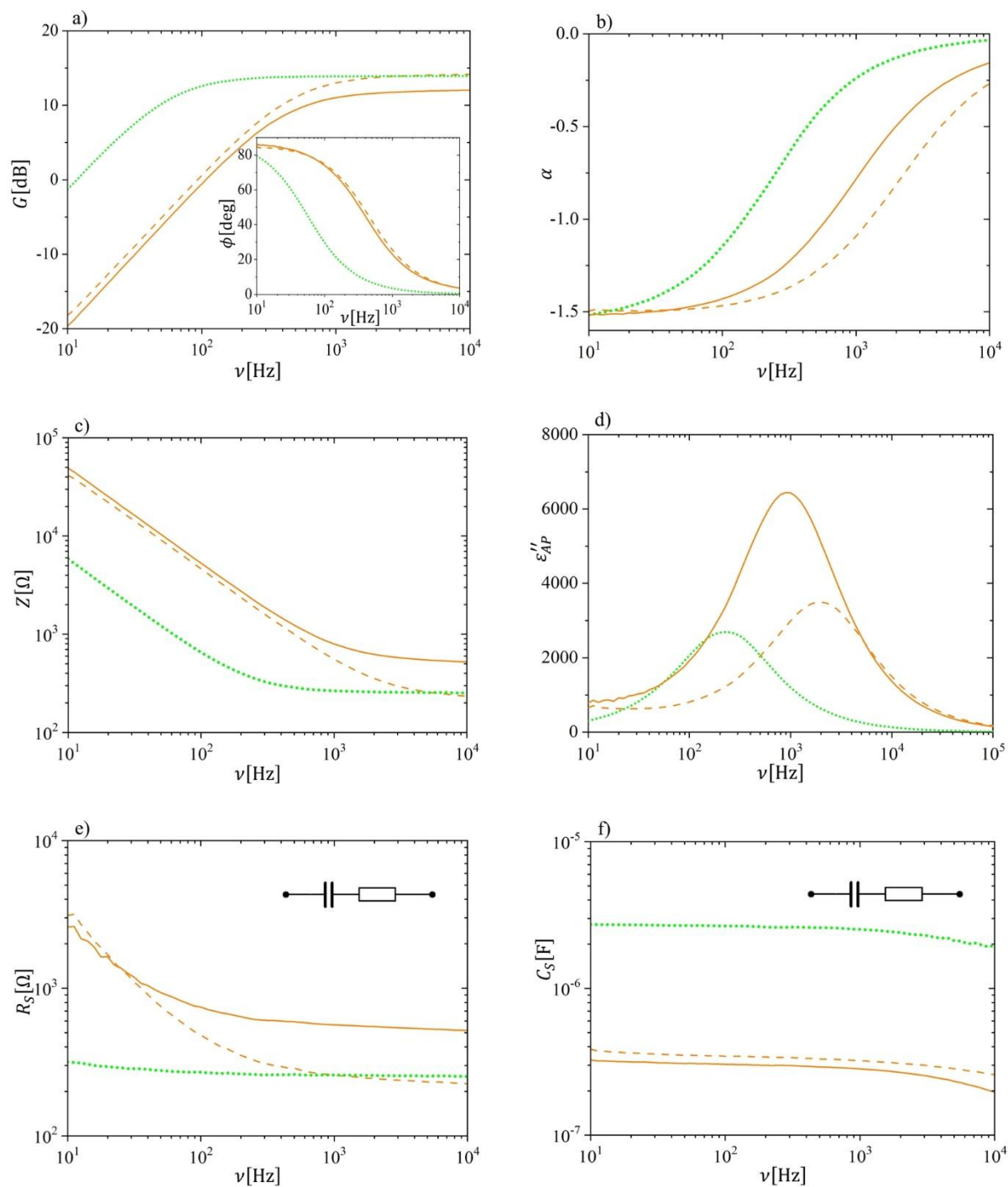


**Figure S5. Material 2** in the  $N_F$  phase at  $80.0^\circ\text{C}$ . **Auto-balancing bridge method.** a) Gain ( $G$ ) and (inset) phase angle ( $\phi$ ) between the voltage on DUT (LC cell and  $R_c$  in series) and current through DUT. b) Phase angle ( $\alpha$ ) between the current through the cell and voltage on the cell and c) impedance  $Z$  calculated from  $G$  and  $\phi$ . d) The apparent dielectric loss calculated by eq. (S14). The apparent e) resistivity ( $R_S$ ) and f) capacitance ( $C_S$ ) of the cell as a function of frequency ( $\nu$ ) by simulating the measured  $Z$  and  $\alpha$  as resulting from a series connection of an ideal resistor and capacitor. Green: NA3. Orange: G10 (solid), G5 (dashed).

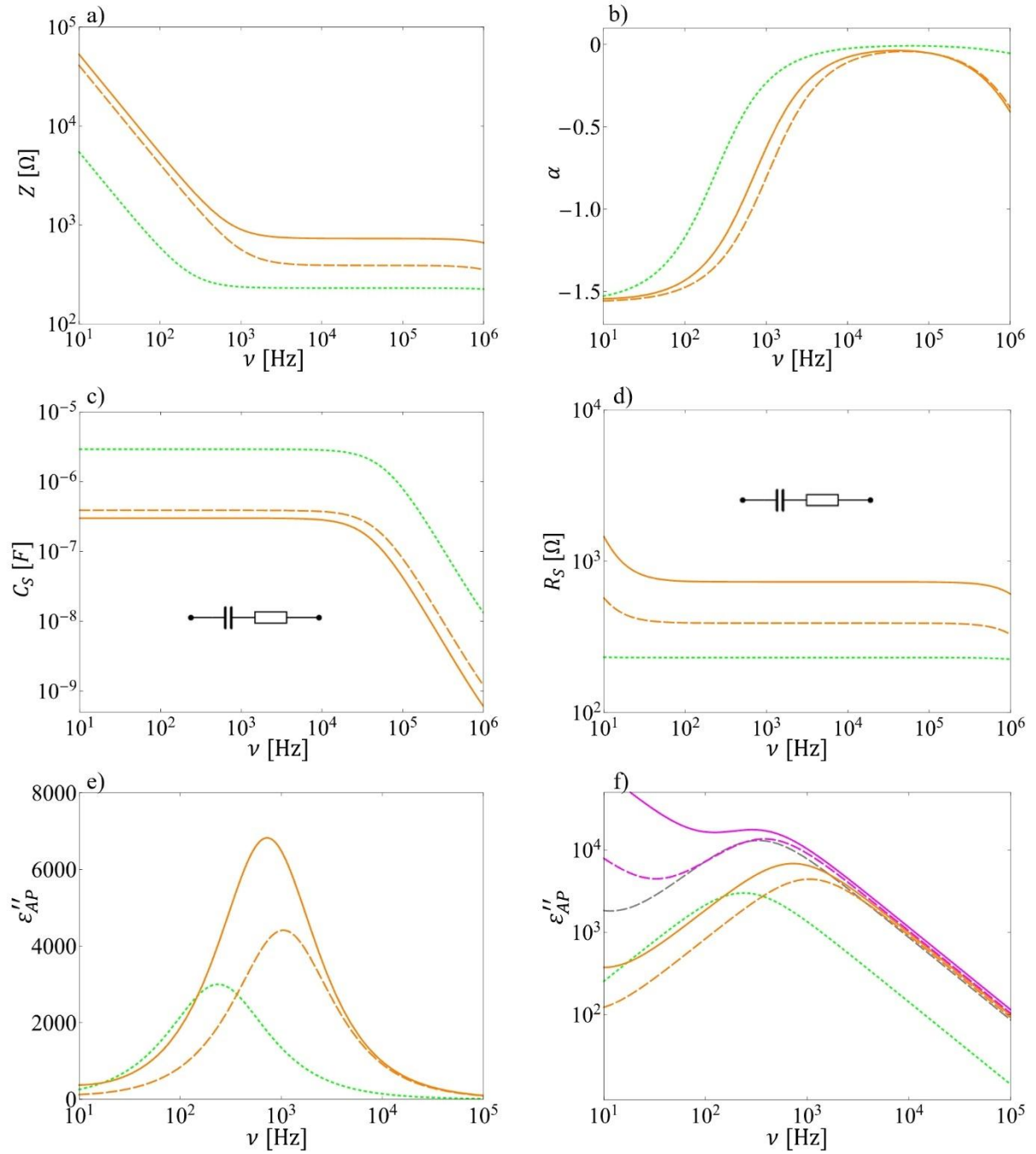


**Figure S6. Material 2. Model results.** a) The impedance ( $Z$ ) and b) phase angle ( $\alpha$ ) between the current through the cell and voltage on the cell as a function of frequency ( $\nu$ ), calculated for the equivalent circuit of the LC cell (Figure 3) with parameters given in Table S1. The apparent c) capacitance ( $C_S$ ) and d) resistivity ( $R_S$ ) of the cell obtained by simulating  $Z$  and  $\alpha$  of the equivalent circuit as resulting from a series connection of a resistor and capacitor. An apparent dielectric loss ( $\epsilon''_{AP}$ ) for e) the measured cells and f) also for thicker cells: 100 nm thick HT cell (magenta, dashed), 1 mm thick HT cell (magenta, solid) and 100 nm thick NA cell (gray, dashed). Green: NA3 (dotted). Orange: G10 (solid), G5 (dashed).

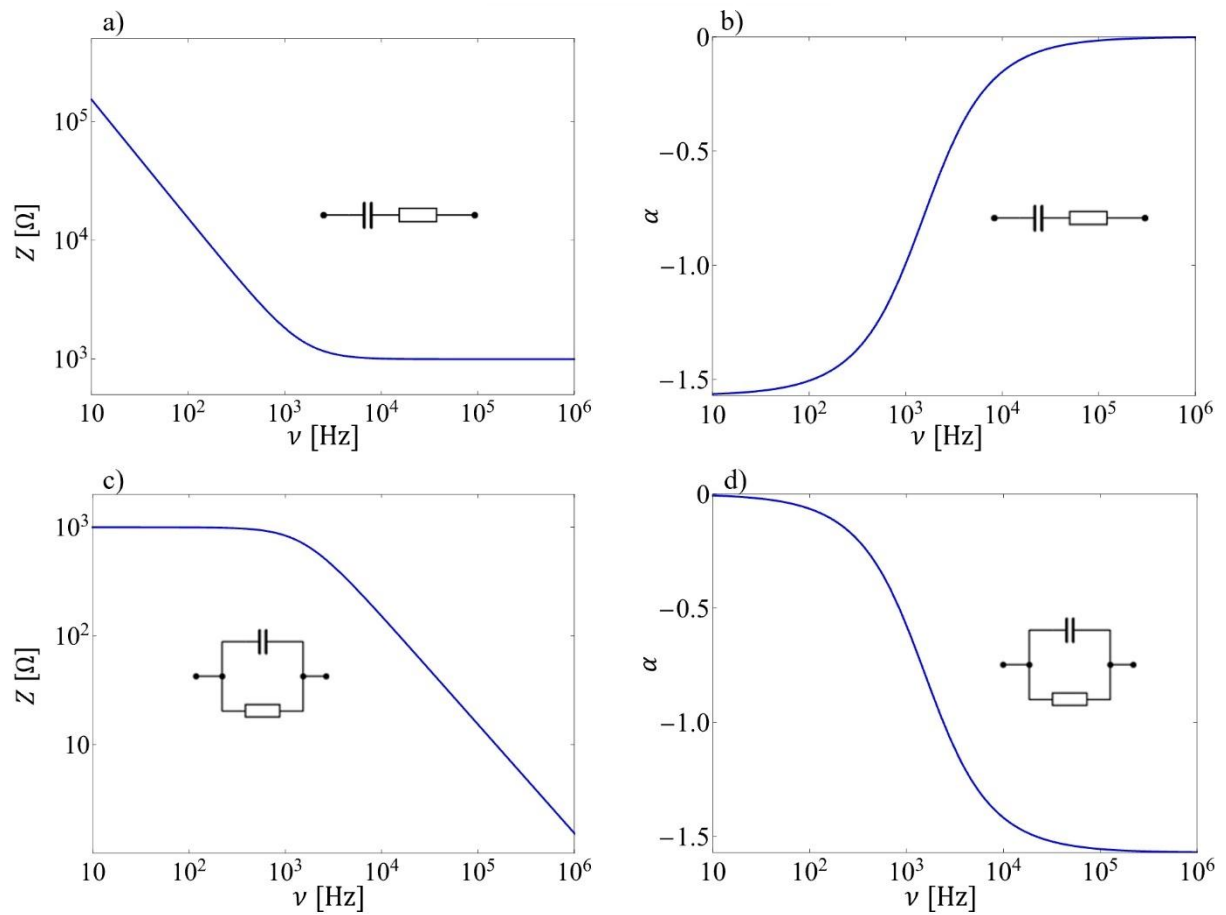


**Figure S7.** A resistor with resistivity  $1 \text{ k}\Omega$  and capacitor with a capacitance  $100 \text{ nF}$  in either a series or parallel connection represent DUT. The frequency ( $\nu$ ) dependence of the a,c) impedance ( $Z$ ) and b,d) angle between the voltage on DUT and current through it.